Vacuum 82 (2008) 1470–1474

Contents lists available at ScienceDirect

Vacuum

journal homepage: www.elsevier.com/locate/vacuum

Effect of the microstructure on the cutting performance of superhard (Ti,Si,Al)N nanocomposite films

C. Fernandes [a], S. Carvalho [a,*], L. Rebouta [a], F. Vaz [a], M.F. Denannot [b], J. Pacaud [b], J.P. Riviére [b], A. Cavaleiro [c]

[a] Dept. Física (GRF), Universidade do Minho, Campus de Azurém, 4800-058 Guimarães, Portugal
[b] Laboratoire de Metallurgie Physique, Université de Poitiers, 86960 Futuroscope, France
[c] ITES – Fac. de Ciências e Tecnologia da Universidade de Coimbra, 3030 Coimbra, Portugal

Keywords:
(Ti,Si,Al)N
Microstructure
HRTEM
XRD

A B S T R A C T

A d.c. reactive magnetron sputtering technique was used to deposit (Ti,Si,Al)N coatings onto WC–Co cutting tools. The microstructure of the coatings was analysed using X-ray diffraction (XRD) and high-resolution transmission electron microscopy (HRTEM) measurement. Before the cutting experiments, the XRD results revealed a structure indexed to an fcc TiN. The results obtained by the XRD tests, with detector variation in asymmetric mode (rocking curves) showed a decrease in the quality of the fiber texture in the (111) grains with the change on deposition chamber geometry (two magnetrons in place of four magnetrons). Cross-sectional HRTEM images of the (Ti,Al)N sample showed grains with a diameter between 16 and 30 nm, while for the (Ti,Si,Al)N samples grains with a diameter between 6 and 10 nm were observed. Furthermore, through the visualization of bright field images it was possible to discern a columnar structure. For samples prepared at high deposition rates (2 μm/h), HRTEM micrographs revealed the formation of the multilayer stacking of (Ti,Si)N/(Ti,Al)N.

1. Introduction

The increasing requirements of high speed and dry cutting applications open up new demands on the quality of cutting tool materials. Traditional hard coatings, such as TiN single layer coatings, played an important role in the development stage in improving the wear resistance of cutting and forming tools. One of the drawbacks of TiN is its limited oxidation resistance to the high temperatures that can be reached during the cutting process. The temperature at the contact between the chip and the tool can rise up to 1200 °C [1,2]. For these extreme cutting conditions (high temperatures/oxidation) chemical resistance is one of the most important requirements for hard coating [3]. Cubic boron, c-BN, nitride coatings have been considered the best solution for cutting applications, such as steel machining, because of their chemical resistance and hardness at high cutting temperatures, [4]. Nevertheless, c-BN deposited by PACVD suffers from high compressive internal stresses that can lead to the premature failure of the tools [5]. (Ti,Al)N coatings can also be an alternative since they exhibit a great improvement in the oxidation resistance, when compared to TiN coatings, as it is possible to use them at temperatures up to 800 °C [6,7]. Thus, the most important criteria for the selection of a coating material for tribological applications include resistance against oxidation, high hardness, high stiffness and a low coefficient of friction. Recently, nanocomposite coatings have attracted increasing interest because of the possibility to combine all of these properties. Among them, coatings of the (Ti,Si)N system are the most studied [8–11], with reports suggesting that that their nanostructure consists of cubic TiN nanocrystallites embedded in an amorphous matrix of silicon nitride. The superhardness of these composites was attributed to the strong resistance of both the crystalline (nc-TiN) and amorphous (a-Si_3N_4) phases having a high cohesive energy at the interface. The usual mechanisms of plastic deformation and crack propagation are absent or hindered, so that mechanical failure in such materials only arises at very high loadings [12]. Previous research with a (Ti,Si,Al)N system [13,14] has demonstrated that these films could belong to this class of nanocomposite materials. It was shown that the hardness increases with a small addition of Si to the (Ti,Al)N system, with the maximum value obtained for a Si content between 2 and 6.5 at.% (values were in the range 45–57 GPa [15]). Also, an increase in the thermal stability of these coatings was observed allowing temperatures over 900 °C to be attained without significant structural transformation [16]. Furthermore, Vaz et al. [17] have shown that a $Ti_{0.27}Al_{0.53}Si_{0.2}N$ coating exhibited better oxidation resistance at 900 °C than a $Ti_{0.35}Al_{0.65}N$ coating.

Also, in previous work [18], nanocomposite (Ti,Si,Al)N and (Ti,Al)N coatings have been deposited onto cermet cutting tools and

* Corresponding author. Fax: +351 253 510 461.
E-mail address: sandra.carvalho@fisica.uminho.pt (S. Carvalho).

0042-207X/$ – see front matter © 2008 Elsevier Ltd. All rights reserved.
doi:10.1016/j.vacuum.2008.03.050

were compared with a commercial coating (one of the best solutions actually available in the market for high speed turning, consisting of a multilayer formed by TiCN, Al_2O_3 and TiN, deposited by thermal CVD, which is only suitable for coating high temperature resistant substrates, such as cemented carbides) used as a reference, when tested in dry cutting operation. The results showed that for high cutting speeds the cutting performance of (Ti,Si,Al)N coated tools could be better than that presented by the commercially available one. Also, the tools coated with (Ti,Si,Al)N showed better cutting performance than the tool coated with (Ti,Al)N. This paper reports the correlation between (Ti,Al,Si)N microstructure and this wear behaviour.

2. Experimental details

2.1. Deposition of the coatings

(Ti,Si,Al)N coatings were deposited on cutting tools of WC–Co by reactive magnetron sputtering, in an Ar/N_2 atmosphere, using a custom made equipment. Rectangular magnetron cathodes of the type 2 were used in a closed field configuration. Two series of samples were produced. Further, detailed information regarding some of the deposition parameters is presented in Table 1, as well as elsewhere [18]. Energy dispersive X-ray spectrometry (EDS), X-ray diffraction (XRD) and high-resolution transmission electron microscopy (HRTEM) were used in order to evaluate the chemical composition, the structure and the microstructure of the coatings, respectively.

3. Results and discussion

3.1. Texture and phase formation – X-ray diffraction analysis

XRD diffraction peaks are displayed in Fig. 1. As discussed in previous works [13–16,18] XRD experiments showed the development of an fcc structure, similar to TiN. Analysis of the figures indicates the presence of a mixture of crystalline phases. For the case of the sample P7-$Ti_{0.56}Al_{0.46}N_{0.98}$ a lattice parameter of 0.419 nm was obtained. This parameter is associated with the formation of a solid solution, where Al atoms replace Ti atoms in TiN cubic lattice, maintaining the fcc structure [19].

When pulverizing using both Ti(Si) and TiAl targets simultaneously, an increase in lattice parameter was observed. In films with a low Al concentration, give rise to the diffraction peaks at lower angles. For a sample produced with the two magnetron configuration (P3 – $Ti_{0.82}Si_{0.08}Al_{0.14}N_{0.96}$ – sample) a lattice parameter of 0.425 nm was found. This must be related with an eventual segregation of Si atoms, which enhances the formation of TiN and Ti(Al)N grains. In fact, if Si atoms were substituting Ti atoms in the TiN lattice, a decrease in the lattice parameter should be observed in relation to the P6 – $Ti_{0.86}Si_{0.04}Al_{0.18}N_{0.92}$ and P10 – $Ti_{0.86}Si_{0.03}Al_{0.16}N_{0.95}$ films, which have a lower Si content (due to the lower atomic radius of Si in comparison to Ti). The presence of segregated Si atoms can be sufficient to nucleate and develop an amorphous matrix of Si_3N_4 [13,14,20]. Thus, the formation of an nc-TiN/a-Si_3N_4/nc-TiAlN should be expected. An Al segregation, with subsequent AlN precipitation, as already reported on (Ti,Al)N films, should not be considered, taking into account the low lattice parameter found for this coating, indicating the presence of Al in solid solution in the cubic TiN lattice [21].The shift observed in the peak position of P3 – $Ti_{0.82}Si_{0.08}Al_{0.14}N_{0.96}$ coated tool, can also be attributed to the compressive residual stress effect [18].

Table 1
Some experimental parameters and properties relative to the sputtered samples

Tool	Composition	Number of magnetrons	J_{TiSi} (mA cm^{-2})	J_{TiAl} (mA cm^{-2})
P3	$Ti_{0.82}Si_{0.08}Al_{0.14}N_{0.96}$	2	10	10
P7	$Ti_{0.56}Al_{0.46}N_{0.98}$	4	0	10
P10	$Ti_{0.86}Si_{0.03}Al_{0.16}N_{0.95}$	4	5	5
P6	$Ti_{0.86}Si_{0.04}Al_{0.18}N_{0.92}$	4	10	10

All the samples were produced with 200 °C as the substrate temperature and with −70 V as bias voltage.

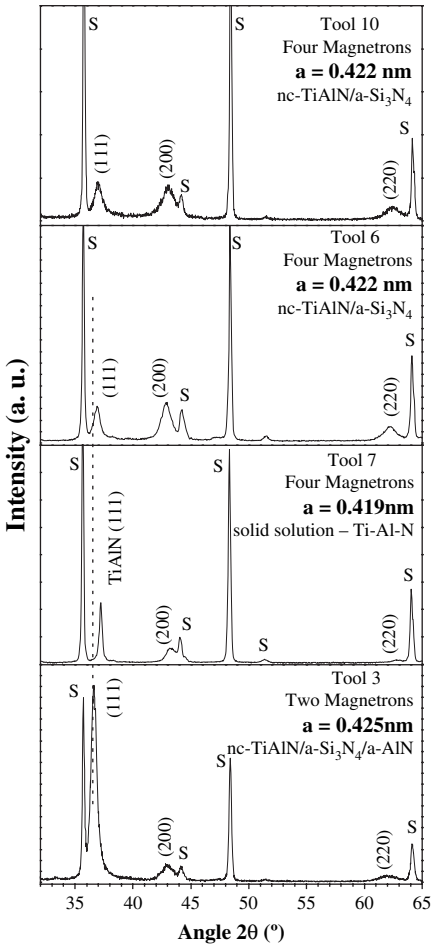

Fig. 1. X-ray diffraction patterns of (Ti,Si,Al)N and (Ti,Al)N films deposited on tungsten carbide substrates.

This sample shows a strong preferential orientation crystallite growth (111), while the other coatings (P7 – $Ti_{0.56}Al_{0.46}N_{0.98}$, P6 – $Ti_{0.86}Si_{0.04}Al_{0.18}N_{0.92}$ and P10 – $Ti_{0.86}Si_{0.03}Al_{0.16}N_{0.95}$) exhibit a decrease in (111) texture, with enhancement of the (200) and (220) crystallite growth. On increasing ion bombardment (by changing the deposition chamber configuration) the surface texture corresponding to the more open crystal channeling direction is favoured. In the case of TiN, the [111] direction exhibits the densest array of atom columns, while the [001] direction is the most open to channeling [22]. It is worth noting that the increase in ion bombardment can be responsible for the lower Si at.% in the P6 – $Ti_{0.86}Si_{0.04}Al_{0.18}N_{0.92}$ and P10 – $Ti_{0.86}Si_{0.03}Al_{0.16}N_{0.95}$ samples, due to the resputtering of this element.

3.2. Fiber texture – rocking curves

The results obtained by the X-ray diffraction tests with detector variation in asymmetric mode (“rocking curves”), for the most intense diffraction region in the diffractograms of the samples, are shown in Fig. 2. Analysis of the data shows that there is a lower quality in the fiber texture of the grains (111) of the samples made

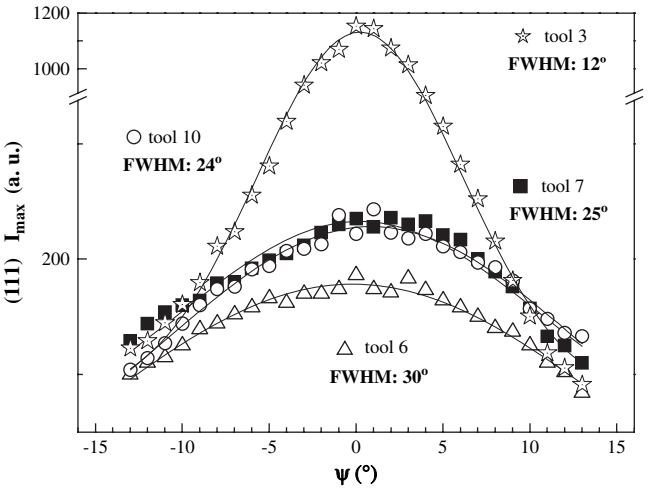

Fig. 2. Rocking curves deduced from detector scans measurements performed on samples showing (111) texture.

with 4 magnetrons (tools 6, 7 and 10). The misorientation of the grains is approximately 13°. The samples made using two magnetrons (tool 3) the misorientation is approximately 6°. These results are in accordance with the strong preferential orientation crystallite growth (111) observed in Fig. 1. The fact that the FWHM is greater than 7° in the samples made with four magnetrons is an indication of the lower texture in the samples, but that does not mean an aleatory growth of the grains. It can be attributed to a rising number of grains growing in the same direction but with a determined inclination to the sample surface.

3.3. High-resolution transmission electron microscopy analysis

By the use of high-resolution transmission electron microscopy (HRTEM), it was possible to analyze the morphology, texture and to estimate the grain size of the samples. A cross-section TEM image of the (TiAl)N sample (P7 – $Ti_{0.56}Al_{0.46}N_{0.98}$) and respective selected area diffraction (SAD) patterns are shown in Fig. 3. This figure shows a dark-field image, indicating a typical columnar grow. It is possible to confirm from the diffraction patterns obtained that this sample is a polycrystalline coating with an fcc structure. The lines illustrated in the inset represent a diffraction ring simulation corresponding to a typical TiN structure, with the lattice parameter obtained by X-ray (0.419 nm). With this image it is possible to distinguish the different rings that correspond to the reflection of most important families' atomic plans found in this sample. The analysis of the Debye–Scherrer rings (see the diffraction patterns in the inset of Fig. 3) also indicates growth on the (111), (200) and (220) planes, which is in agreement with XRD results.

A closer look at Fig. 4 (HRTEM image for P7 – $Ti_{0.56}Al_{0.46}N_{0.98}$ sample) reveals that crystallites with sizes of 16 and 30 nm can be distinguished. However, one must be careful in distinguishing large grains from clusters of extremely fine grains in close crystallographic orientation, since the grain boundaries can be difficult to discern.

The TEM results show that the P10 – $Ti_{0.86}Si_{0.03}Al_{0.16}N_{0.95}$ sample also presented a columnar structure, a feature which is typical of coatings grown under low energetic ion bombardment and limited adatom mobility conditions [23]. It was observed that the column diameter increases with increasing film thickness, therefore, this broadening can be explained by considering the three stages of development of textures in PVD coatings, which are nucleation, competitive growth and steady growth [24].

In Fig. 5, the selected area diffraction (SAD) patterns, for the P10 – $Ti_{0.86}Si_{0.03}Al_{0.16}N_{0.95}$ sample, confirm the formation of an fcc structure, as well as the existence of grains with growth (111), (200) and (220) parallel in orientation to the surface of substrate. This behaviour agrees with the XRD, where only these three reflections were detected. From the rings in the SAD patterns of the polycrystalline sample, it is also possible to identify the formation of two groups of grains. In one group, the grains are orientated relative to the preferential direction of growth with a misorientation *ca.* 15°, and in the other group, the grains are more randomly distributed. The arcs in the SAD pattern are typical of a nanocrystalline structure. This is in agreement with the HRTEM micrograph presented in Fig. 6 for P10 – $Ti_{0.86}Si_{0.03}Al_{0.16}N_{0.95}$ sample. In fact, the nanocrystalline nature of the (Ti,Al)N grains is revealed by a dispersion of the grain sizes between 6 and 10 nm, although these differences can also relate to the possible superposition of different grains. In the case of films deposited with the same geometrical arrangement, the addition of Si gives rise to a reduction in the grain size (comparing tool 7 and tool 10 samples). When there is sufficient surface mobility, silicon can segregate towards the grain boundaries of the transition-metal nitride and nucleate a Si–N phase. The presence of this amorphous phase can contribute to the fixing of the boundaries of the nanocrystallites, thus, limiting their growth [25,26].

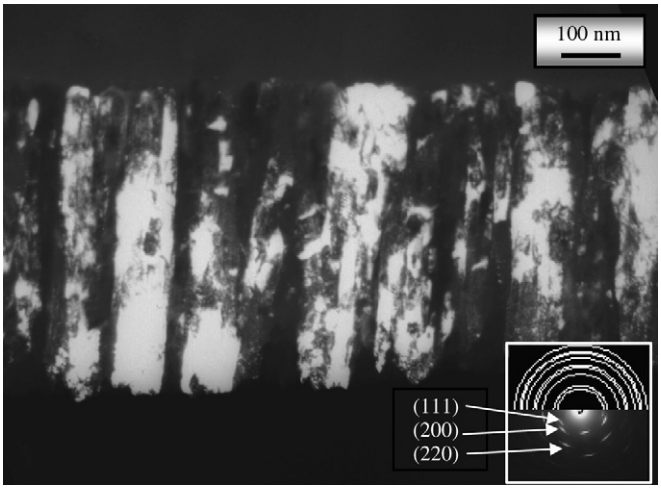

Fig. 3. Dark-field TEM micrograph from the cross-section of P7 – $Ti_{0.56}Al_{0.46}N_{0.98}$ tool. The inset shows a selected area diffraction pattern (SAD).

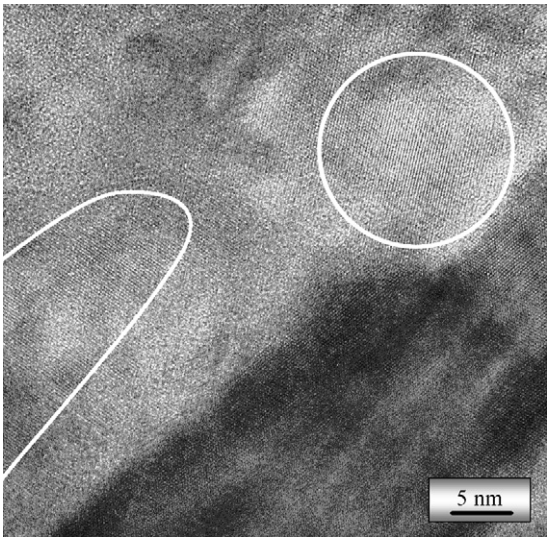

Fig. 4. HRTEM micrograph from the cross-section of the $Ti_{0.56}Al_{0.46}N_{0.98}$ sample.

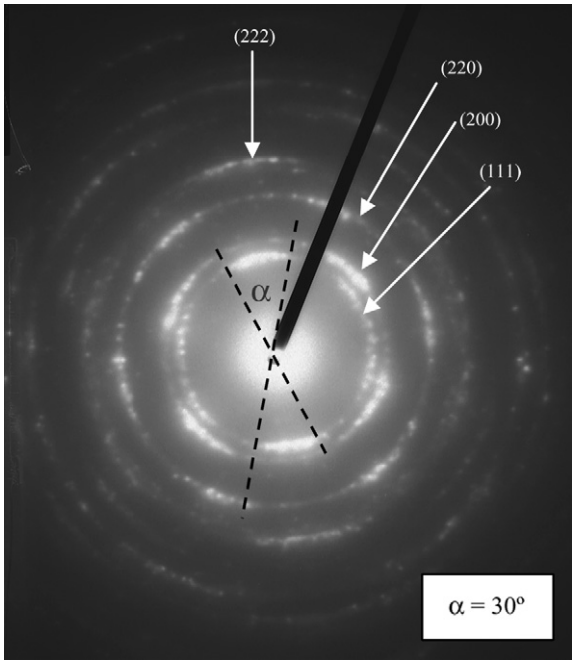

Fig. 5. Selected area diffraction pattern of $Ti_{0.86}Si_{0.03}Al_{0.16}N_{0.95}$.

For a constant substrate rotation speed, when the deposition rates are sufficiently high, as is the case for P3 – $Ti_{0.82}Si_{0.08}Al_{0.14}N_{0.96}$ sample, the use of (Ti,Al) and (Ti,Si) targets in opposition arrangement, promotes an alternate deposition that results in a multilayer of (Ti,Si)N/(Ti,Al)N type. This film was produced with a modulation period (Λ) of 4.7 nm, as shown in the HRTEM micrograph in Fig. 7. In this particular case the sample was grown with a deposition rate of 2 μm/h. Further detailed information regarding the presence of this multilayer growth can be found elsewhere [27].

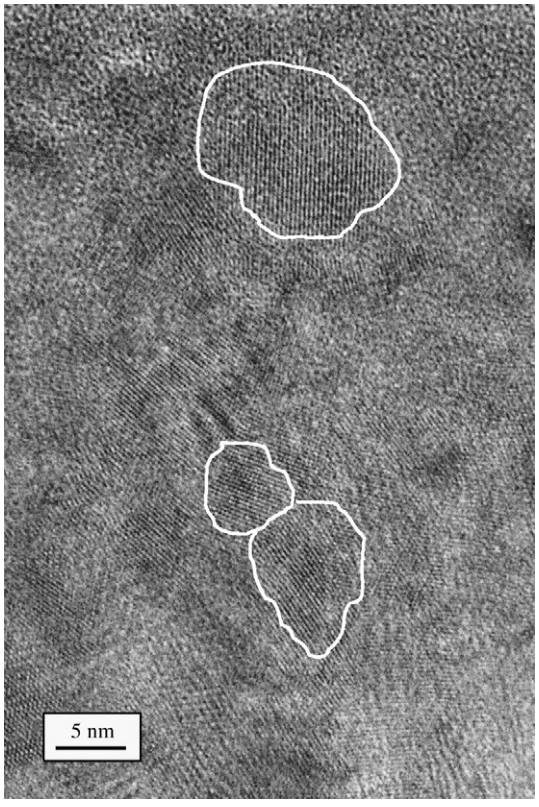

Fig. 6. HRTEM micrograph from the cross-section of the $Ti_{0.86}Si_{0.03}Al_{0.16}N_{0.95}$ sample.

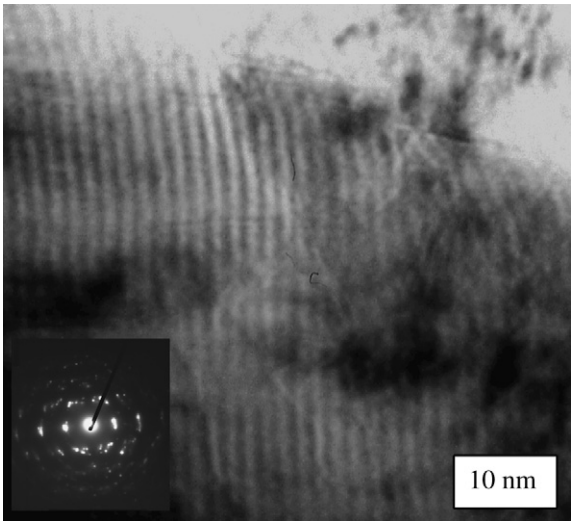

Fig. 7. HRTEM micrograph from the $Ti_{0.82}Si_{0.08}Al_{0.14}N_{0.96}$ sample, showing a (Ti,Si)N/(Ti,Al)N multilayer stacking with $\Lambda = 4.7$ nm. A selected area diffraction pattern (SAD) corresponding to this zone is in the inset.

4. Conclusion

The performance of the Ti–Al–N (P7 – $Ti_{0.56}Al_{0.46}N_{0.98}$ sample – solid solution) coating is worst at high cutting speed compared with the nc-(Ti,Al)N/a-SiN_x coating. Because of an enhancement in nanocrystal/amorphous phase segregation it is more favorable to machine the work-pieces. However, the tribological performance of (Ti,Al,Si)N coatings to cutting tools only partially correlates with this structural arrangement. In the literature, large improvements in wear properties were reported for multilayered coatings, compared with the single-layer coatings. In fact, the increase in the wear behaviour of the P3 – $Ti_{0.82}Si_{0.08}Al_{0.14}N_{0.96}$ coating can be related with the development of a multilayer system, as detected by HRTEM results.

References

[1] Buljan ST, Wayne SF. Wear 1989;133:309.
[2] Silva RF, Gomes JM, Miranda AS, Vieira JM. Wear 1991;148:69.
[3] Wittmer M, Nose J, Melchior H. J Appl Phys 1981;52:6659.
[4] Holubar P, Jilek M, Sima M. Surf Coat Technol 1999;120–121:184.
[5] Yoshida T. Diamond Relat Mater 1996;5:501.
[6] McIntyre D, Greene JE, Hakansson G, Sundgren JE, Munz WD. J Appl Phys 1990;67:1542.
[7] Hofmann S, Jehn HA. Surf Interface Anal 1988;12:329.
[8] Veprek S. Surf Coat Technol 1997;97:15.
[9] Mitterer C, Mayrhofer PH, Beschliesser M, Losbichler P, Warbichler P, Hofer F, et al. Surf Coat Technol 1999;120–121:405.
[10] Sun X, Reid JS, Kolawa E, Nicolet M-A. J Appl Phys 1997;81(2):656.
[11] Vaz Filipe. Preparação e caracterização de revestimentos duros nano-estruturados de $Ti_{1-x}Si_xN_y$, preparados por pulverização catódica reactiva em magnetrão, tese de doutoramento. Univeridade do Minho; 2000.
[12] Niederhofer A, Nesládek P, Männling H-D, Moto K, Veprek S, Jílek M. Surf Coat Technol 1999;120–121:173.
[13] Carvalho S, Vaz F, Rebouta L, Schneider D, Cavaleiro A, Alves E. Surf Coat Technol 2001;142–144:110.
[14] Ribeiro E, Malczyk A, Carvalho S, Rebouta L, Fernandes JV, Alves E, et al. Surf Coat Technol 2002;151–152:515.
[15] Carvalho S, Ribeiro E, Rebouta L, Pacaud J, Goudeau Ph, Renault PO, et al. Surf Coat Technol 2003;172:109–16.
[16] Carvalho S, Rebouta L, Cavaleiro A, Rocha LA, Gomes J, Alves E. Thin Solid Films 2001;398–399:391–6.
[17] Vaz F, Rebouta L, da Silva MF, Soares JC. In: Pauleau Y, Barna PB, editors. Protective coatings and thin films; 1997. p. 501.

[18] Carvalho S, Ribeiro E, Rebouta L, Tavares C, Mendonça JP, Caetano Monteiro A, et al. Surf Coat Technol 2004;177–178:459.
[19] Knotek O, Böhmer M, Leyendecker T. J Vac Sci Technol A 1986;4(6):2695.
[20] Vaz F, Rebouta L, Almeida B, Godeau P, Pacaud J, Riviere JP, et al. Surf Coat Technol 1999;120–121:166.
[21] Musil J, Hrubý H. Thin Solid Films 2000;365:104.
[22] Petrov I, Adibi F, Greene JE, Hultman L, Sundgren JE. Appl Phys Lett 1993; 63:36.
[23] Thornton AJ. J Vac Sci Technol A 1986;4:3059.
[24] Carvalho NJM, DeHosson J Th M. Thin Solid Films 2001;388:150.
[25] Barna PB, Adamik M, Lábár J, Köver L, Tóth J, Dévényi A, et al. Surf Coat Technol 2000;125:147.
[26] Durand-Drouhin O, Santana AE, Karimi A, Derflinger VH, Schütze A. Surf Coat Technol 2003;163–164:260.
[27] Carvalho Sandra. Propriedades mecânicas e características microestruturais de filmes finos nanocompósitos de (Ti,Al,Si)N preparados por pulverização catódica reactiva em magnetrão, tese de doutoramento. Univeridade do Minho; 2004.